Molecular Dynamics Study of Dendrimers: Structure and Effective Interaction

Takamichi Terao* and Tsuneyoshi Nakayama

Department of Applied Physics, Hokkaido University, Sapporo 060-8628, Japan

Received June 23, 2003; Revised Manuscript Received February 9, 2004

ABSTRACT: We report the results of stochastic molecular dynamics simulations for the structural formation of charged dendrimers and dendrimer-based star polymers. The variation in the radius of gyration explains quite well recent small-angle neutron-scattering experiments for higher-generation charged dendrimers under different pH conditions. We also clarify the properties of effective interaction between dendrimers for weak and strong electrostatic couplings in an aqueous solution.

Introduction

Many kinds of dendrimers, with different initiator cores and branches, have been synthesized in this decade, for which intensive studies have been performed on their practical use as a new functional material in biochemical and medical applications.[1−5] Dendrimers have numerous potential applications such as utilizing their inner space (i.e., nanosized molecular encapsulation) in drug-delivery systems, and as contrast agents for visualizing blood vessels and bloodstreams in magnetic resonance imaging(MRI).[6−9]

It is quite significant to understand the conformation of dendrimers in solution for their application as nanocapsules. Dendrimers are formed by a step-by-step iterative reaction starting from a core. The resulting treelike molecules have a well-defined number of end groups and narrow molecular weight distributions. A key problem is their spatial structures and the location of the end groups. Small-angle neutron scattering (SANS) and small-angle X-ray scattering (SAXS) experiments have been performed in order to elucidate the spatial structure of dissolved dendrimers.[10−14] SANS is the optimal tool for probing the location of end groups, because their contrast can be greatly enhanced using the deuterium labeling technique. Recently, SANS studies have been conducted to discuss the gyration radius of dendrimers bearing deuterated end groups.[15−17] The experiments have revealed that the conformation and the gyration radius of dendrimers change as a function of the pH condition and the ionic strength of the solution. On the contrary, Nisato et al.[17] have reported results of SANS experiments on G8 PAMAM dendrimers, claiming that the gyration radius does not depend on the pH condition of the solution. These results indicate that the structural changes become negligible in higher-generation dendrimers. Thus, a definite conclusion about the size variation of dendrimers is still unclear.

We present the results of stochastic molecular dynamics simulations in order to reveal the nanosized structural formation of charged dendrimers, and dendrimer-based star polymers in solution.[18,19] We calculate the gyration radius, density distribution function, and the structure factor of these systems under different pH conditions, ionic strengths, and number of generations. In addition, the effective interaction between dendrimer molecules is investigated numerically. The results show that the effective force between dendrimers is repulsive with weak electrostatic couplings and is inversely proportional to the distance between molecules.

This paper is organized as follows. In section 2, we describe the model of polyelectrolyte dendrimers in solution. Section 3 reports the numerical results on the conformation of polyelectrolyte dendrimers and dendrimer-based star polymers in solution. We also discuss the variation of the gyration radius in detail. The effective interaction between dendrimers in an electrolyte solution is presented in section 4. The conclusions are given in section 5.

2. Models

We study the conformation of dendrimers in a solution by using the stochastic molecular dynamics simulations.[20] The solvent is treated as a continuum, which acts as a heat bath for the molecules and produces a viscous drag when each segment moves. The equation of motion for the ith segment with mass m is given by

$$m\frac{\mathrm{d}^2}{\mathrm{d}t^2}\boldsymbol{r_i}(t) = -\nabla U_{\mathrm{i}} - m\Gamma\frac{\mathrm{d}}{\mathrm{d}t}\boldsymbol{r_i}(t) + \boldsymbol{W_i}(t) \qquad (1)$$

where Γ, $\boldsymbol{r_i}(t)$, and $\boldsymbol{W_i}(t)$ are the friction coefficient that couples the monomers to the heat bath, the positional vector of the ith segment, and the random force of the heat bath acting on each segment, respectively. $\boldsymbol{W_i}(t)$ is a Gaussian white noise such as

$$\langle \boldsymbol{W_i}(t)\cdot\boldsymbol{W_j}(t')\rangle = 6mk_{\mathrm{B}}T\Gamma\delta_{ij}\delta(t-t') \qquad (2)$$

where k_{B} is the Boltzmann constant and T is the temperature of the system. The potential U_i consists of three terms, and is given by

$$U_i = \sum_j U_{\mathrm{LJ}}(r_{ij}) + U_{\mathrm{FENE}} + U_{\mathrm{c}} \qquad (3)$$

where r_{ij} is the distance between monomers i and j. Here $U_{\mathrm{LJ}}(r)$ is a Lennard-Jones potential between any two monomers written as

* Corresponding author. E-mail terao@eng.hokudai.ac.jp.

10.1021/ma030349h CCC: $27.50
Published on Web 05/12/2004

$$U_{\mathrm{LJ}}(r_{ij}) = \begin{cases} 4\epsilon\left[\left(\frac{\sigma}{r_{ij}}\right)^{12} - \left(\frac{\sigma}{r_{ij}}\right)^{6} - \left(\frac{\sigma}{r_c}\right)^{12} + \left(\frac{\sigma}{r_c}\right)^{6}\right] & \text{for } r_{ij} \le r_c \\ 0 & \text{for } r_{ij} > r_c \end{cases} \quad (4)$$

where ϵ, σ and r_c are the unit of energy, the diameter of particles, and the cutoff radius, respectively, and r_c is taken as $r_c = 2.5\sigma$. U_{FENE} denotes the bonding interaction between neighboring segments, which is given by

$$U_{\mathrm{FENE}}(r_{ij}) = \begin{cases} -0.5KR_0^2 \ln\left[1 - \left(\frac{r_{ij}}{R_0}\right)^2\right] & \text{for } r_{ij} \le R_0 \\ 0 & \text{for } r_{ij} > R_0 \end{cases} \quad (5)$$

where K is a bonding constant and R_0 is the maximum extension of the bond. In the following simulation, we use the values $R_0 = 1.5\sigma$ and $K = 30.0\epsilon/\sigma^2$, since these parameters prevent bond crossings. U_c is the screened Coulomb potential between monomers with charge $z_i e$ and $z_j e$ given by

$$\frac{U_c(r_{ij})}{k_B T} = \lambda_B \frac{z_i z_j}{r_{ij}} \exp(-\kappa r_{ij}) \quad (6)$$

where $\lambda_B = e^2/4\pi\tilde{\epsilon}k_B T$ is the Bjerrum length ($\tilde{\epsilon}$ is the dielectric constant of the medium), and κ is the inverse Debye screening length depending on the ionic strength such as

$$\kappa = \sqrt{4\pi\lambda_B \sum_j c_j q_j^2} \quad (7)$$

Here c_j and q_j are the concentration and valence of the jth ion in solution, respectively. We have to mention that these numerical treatments (eq 6) can be justified only when the electrostatic coupling is sufficiently weak. When the electrostatic coupling is strong, counterion condensation effect becomes important, and the Debye−Hückel approximation is not valid any more. We will explain the numerical treatment for such cases in section 4.

In the following, we consider three different models to treat the effect of pH conditions on polyelectrolyte dendrimers such as poly(amidoamine) (PAMAM) dendrimers. Under a high pH condition, no amines are assumed to be protonated.[21] Under a neutral pH condition, all the primary amines of a dendrimer molecule are protonated (shown as black circles in Figure 1), and under a low pH condition, all the amines are protonated (shown as black and hatched circles in Figure 1). The initial configuration of dendrimer molecules is built as follows: The segment of each chain is attached by self-avoiding random walks with a distance of $\sim\sigma$ in a cubic box of system size L. A dendrimer with G generation is built by adding $M_b - 1$ chains (of length M_n) to each of the free ends of a dendrimer with $G - 1$ generation, where M_b and M_n are the branching factors and the length per monomer between each branching point, respectively. The same procedure is continued in order to build dendrimers of desired generation numbers. The temperature T and the friction coefficient Γ are taken to be $k_B T/\epsilon = 1.2$ and $\Gamma = 0.5\tau^{-1}$, respectively, and a time step $\delta t = 0.001\tau$ or $\delta t = 0.002\tau$ is selected, where τ is the unit of time defined as $\tau \equiv \sigma(m/\epsilon)^{1/2}$. In actual calculations, we carry out the Monte Carlo(MC) simulation with short MC steps($\sim 10^4$ MCS) for structural relaxation, prior to molecular dynamics(MD) simulations. In the MD simulation, physical quantities are calculated after a sufficient number of MD steps are discarded to reach an equilibrium. The equations of motion (eq 1) are integrated using a velocity−Verlet algorithm. These MC and MD codes are parallelized efficiently using the message-passing interface (MPI). The parameters used in this study are summarized in Table 1.

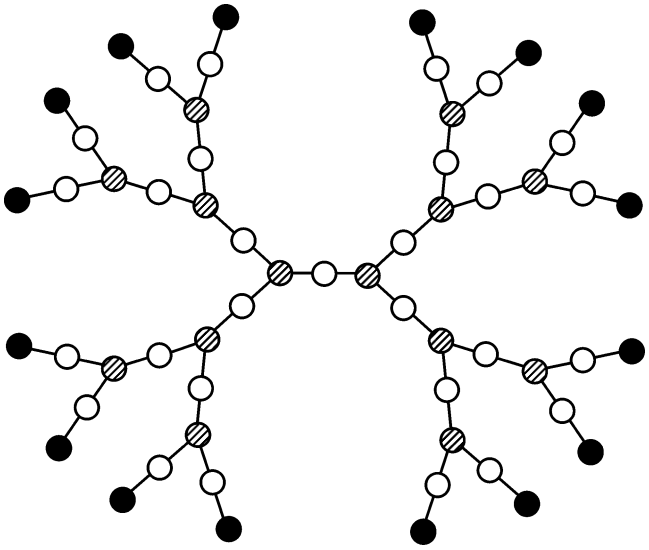

Figure 1. Model of dendrimers in solution. Solid circles, hatched circles, and open circles are explained in the text.

Table 1. Simulation Parameters in Molecular Dynamics Simulation

generation	M_n	L/σ	N
G5	2	40.0	507
G5	4	40.0	1013
G6	4	40.0	2037
G7	2	60.0	2043
G7	1	40.0	1022

3. Numerical Results

3.1 Structural Formation of Dendrimers. At first, we calculate the gyration radius $R_g = R_g(t)$ and the autocorrelation function $C_R = C_R(t)$ of G5 dendrimers, to verify whether time steps taken to observe the equilibrium states are sufficiently long in the MD simulations. The autocorrelation function $C_R(t)$ is defined by

$$C_R(t) \equiv \frac{\langle [R_g^2(t) - \langle R_g^2 \rangle][R_g^2(0) - \langle R_g^2 \rangle] \rangle}{\langle R_g^4 \rangle - \langle R_g^2 \rangle^2} \quad (8)$$

Figure 2 shows the time development of the gyration radius $R_g(t)$ under a low pH condition. The Debye screening length κ^{-1} is set to be $\kappa^{-1} = 10.0\sigma$. The inset of Figure 2 shows the result of the autocorrelation function $C_R(t)$. In Figure 2, the value of the gyration radius $R_g(t)$ reaches an equilibrium after long time steps. These results confirm that when the relaxation time τ is defined by $C_R(t = \tau) \sim 1/e$, the time steps taken are sufficiently long ($t \gg \tau$). Parts a and b of Figure 3 are snapshots of G5 dendrimers with screening length $\kappa^{-1} = 1.0\sigma$ and 10.0σ, respectively. In Figure 3a, a dendrimer molecule takes a spherical form, and it shows a drastic structural change under different solvent conditions.

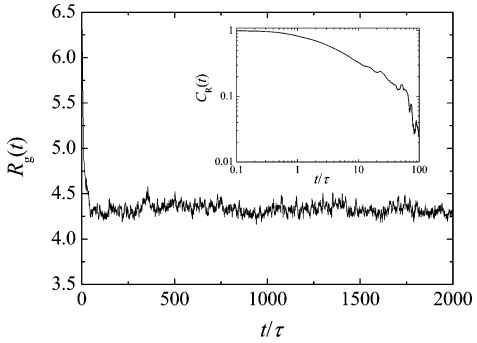

Figure 2. Time development of the gyration radius $R_g(t)$ with G5 dendrimers. Inset shows the calculated result of the autocorrelation function $C_R(t)$.

In recent studies, SANS and SAXS experiments have been performed to clarify the structural formation of dendrimers in solution.[10−12] The structure factor $S(q)$ is defined by

$$S(\boldsymbol{q}) \equiv \frac{1}{N}\left|\sum_{i=1}^{N} e^{i\mathbf{q}\cdot\mathbf{r}_i}\right|^2 \tag{9}$$

where N, $\boldsymbol{r_i}$ and $\boldsymbol{q}$ are the number of segments, the positional vector of ith segment, and the scattering vector, respectively. Here $\boldsymbol{q}$ obeys the following expression

$$|\boldsymbol{q}| = \frac{4\pi}{\lambda}\sin\left(\frac{\theta}{2}\right) \tag{10}$$

where θ and λ denote the scattering angle and the wavelength of the incident beam, respectively. We calculate the wavenumber dependence of the structure factor $S(q)$ numerically, to compare with the SANS experimental results. The results of the structure factor $S(q)$ are shown in Figure 4. The wavenumber dependence of the structure factor $S(q)$ oscillatory decays, and its profile has a local minimum. These features agree well with previous experiments, as shown in Figure 2 of ref 17. Parts a and b of Figure 4 display the dependence of the structure factor $S(q)$ on ionic strengths and pH conditions, respectively. In each figure, the characteristic wavenumber on the solid line (shown by vertical arrow) shifts to a lower wavenumber regime, thus reflecting an increase in the gyration radius R_g. In Figure 2 of ref 17, there is a local maximum located at the smaller wavenumber for the low-screened condition, and this feature is absent in Figure 4. This discrepancy is due to the fact that the local maximum located at the smaller wavenumber may be caused by the repulsion between dendrimers, especially for low-screened conditions. In this study, we treat only a single dendrimer molecule, and it is the future problem to confirm this issue by molecular dynamics simulation, treating a lot of dendrimer molecules in an aqueous solution.

3.2 Comparison with the SANS Experiments. The location and the spatial distribution of end groups are important issues because various functional groups and other molecules are attached to the terminal parts of a dendrimer. Among various theoretical approaches, one starts with the assumption that all branches extend to the periphery of the dendrimer molecule due to steric interactions between the end groups (dense-shell picture), and these branches form a hollow core with small segment density in the center of the molecule. Another has predicted that the segment distribution function is the maximum at the center of the molecules (dense-core picture). The dense-core picture assumes that a part of the end groups are folded back into the interior of the molecule and are dispersed throughout the structure of the dendrimers.

Lyulin, Davies, and Adolf[22] have argued about the interpretation of SANS experiments with deutrium labeling[15] to characterize the spatial distribution of perimeters. The relative difference of the gyration radius ΔR is defined by[22]

$$\Delta R \equiv \frac{R_g^{(\mathrm{peri})} - R_g}{R_g} \tag{11}$$

Here R_g is the gyration radius of a dendrimer, and $R_g^{(\mathrm{peri})}$ is the gyration radius of deuterated terminal units. Table 2 shows the calculated results of the gyration radii R_g and $R_g^{(\mathrm{peri})}$, and the difference of the radius ΔR under different conditions. Although R_g and $R_g^{(\mathrm{peri})}$ are sensitive to the properties of solutions, it is assumed that ΔR takes a constant value $\Delta R = 0.11 \sim 0.12$, irrespective of pH conditions, ionic strengths, and the generation of the system. These results demonstrate that the value of ΔR in eq 11 does not reflect the structural change of dendrimers in solution.

A SANS experiment by Chen et al.[16] has reported that the conformation and the gyration radius of dendrimers varies as a function of pH conditions and ionic strengths of the solution. Nisato et al.[17] have made the SANS experiment on G8 PAMAM dendrimers and have concluded that the size of a dendrimer is essentially independent of the solvent conditions. The results of the experiment performed by Nisato et al.[17] imply that the structural changes become negligible in higher generation dendrimers, which at first glance, seems contrary to the previous experiments by Chen et al.[16] and computer simulations by Welch and Muthukumar[23] and Lee et al.[24] We calculate the gyration radius R_g and density distribution function of dendrimers under different solvent conditions to reveal the detailed structure of dendrimers, and interpret the experimental results.[16,17] Figure 5 gives the density distribution function in the case of two different generations (G5 and G7). The calculated results are averaged over time in the MD simulations. As shown in Figure 3 of ref 17, the profile of $r^2n(r)$ agrees well with that of the distance distribution function of PAMAM. Figure 5a shows the pH dependence of $r^2n(r)$ and $r^2n_{\mathrm{peri}}(r)$ on G5 dendrimers ($M_n = 4$). The profile of $r^2n(r)$ changes as a function of pH conditions in the solution, which is in agreement with the previous Monte Carlo studies by Welch and Muthukumar.[23] It becomes clear that, under a high pH condition, the spatial distribution of perimeter segments is not localized outward, but dispersed inside the dendrimer molecule. Figure 5b displays the pH dependence of distribution function $r^2n(r)$ on higher generation dendrimers. Compared with Figure 5a, the peak position of the density distribution function $r^2n(r)$ becomes less sensitive to pH conditions in solution. Table 3 summarizes the results of the gyration radius of G7 dendrimers. We find that the pH dependence of the gyration radius R_g becomes small in the case of $M_n = 1$. This is due to the steric effect between segments in higher generation system having a small free-volume, and thus it explains the recent SANS experiments by

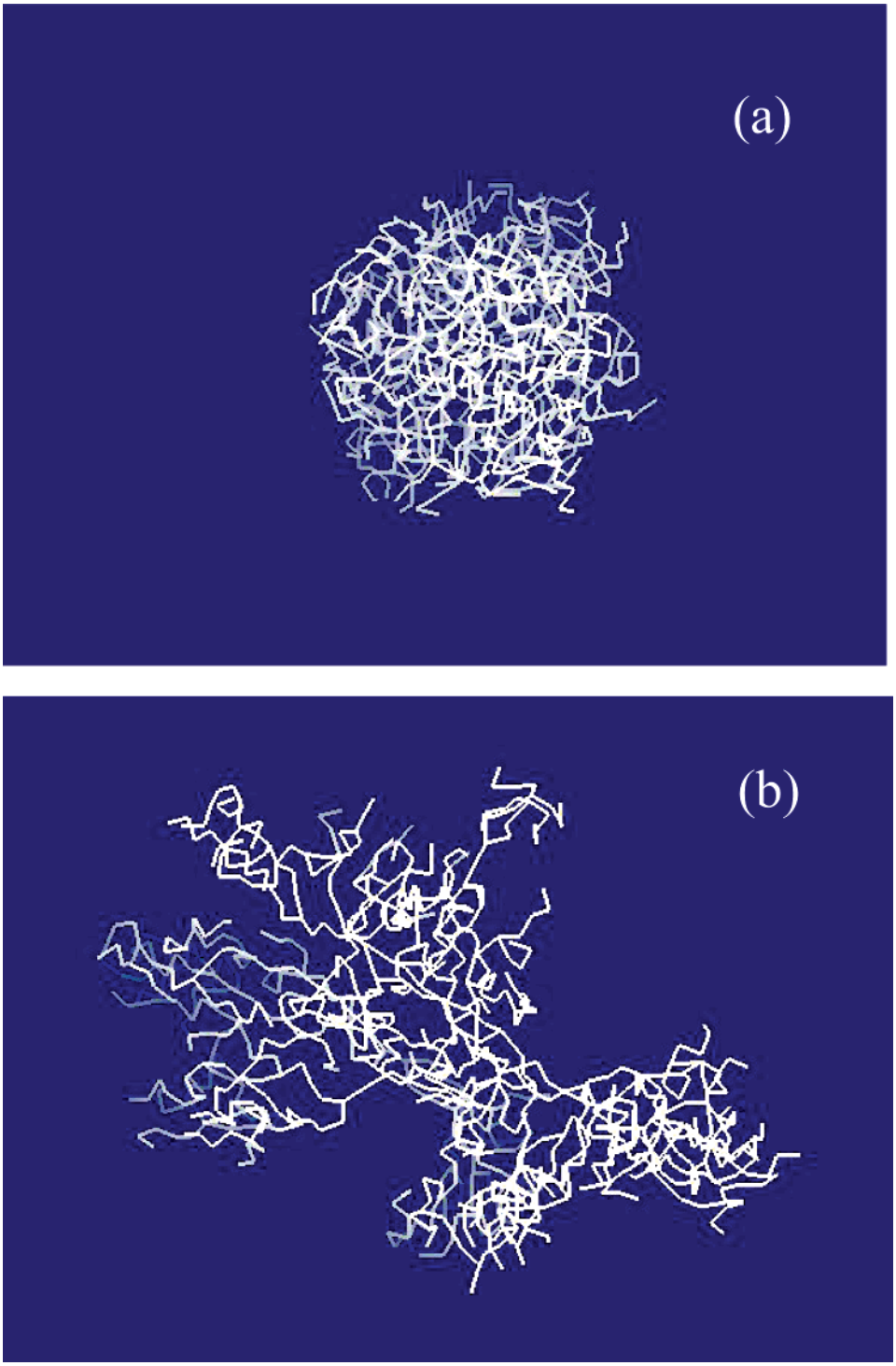

Figure 3. Snapshot of G5 dendrimers under low pH condition. (a) The Debye screening length $\kappa^{-1} = 1.0\sigma$. (b) $\kappa^{-1} = 10.0\sigma$.

Nisato et al.[17] In ref 25, Timoshenko, Kuznetsov, and Connolly have performed detailed studies on the conformation of dendrimers. They have confirmed that while smaller dendrimers have a dense core, larger ones develop a hollow domain.[25] Figure 5b implies that our results shows good agreement with the results in ref 25, because the values of $r^2n(r)$ under low pH condition (open triangles) in Figure 5b are shown to be zero for $r/\sigma \leq 5$.

3.3 Conformation of Dendrimer-Based Star Polymers. Dendrimer-based star polymers are regarded as block copolymers between globular dendrimers and linear polymers. These are expected to play an important role as novel functional materials in biochemistry. In recent studies, a variety of polymer-substituted dendrimers have been synthesized. A typical example is *sugar balls*—full sugar-substituted globular dendrimers.[18] Sugar balls consist of an internal dendrimer skeleton covered with an external sugar layer, and they are applications of the functionalization of dendrimers as a result of the recent progress in glycotechnology. Such artificial glycoconjugates with molecular recognition ability are indispensable for many biomedical applications. Another example of dendrimer-based star polymers is water-soluble poly(ethylene glycol) (PEG) dendrimers.[19,26]

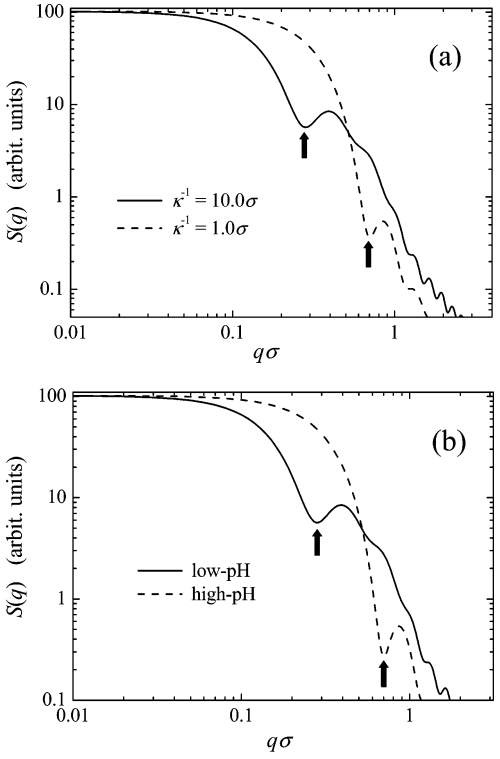

Figure 4. (a) Salt dependence on the structure factor $S(q)$ of G5 dendrimers. Solid line and dashed line denote the calculated results with the screening length $\kappa^{-1} = 10.0\sigma$ and 1.0σ, respectively. (b) pH dependence on the structure factor $S(q)$. Solid line and dashed line denote the calculated results under low pH and high pH conditions, respectively.

Table 2. Results of the Gyration Radius of Dendrimer

generation	pH	M_n	$(\kappa\sigma)^{-1}$	R_g/σ	$R_g^{(peri)}/\sigma$	ΔR
G5	high	2		4.19	4.72	0.13
G5	neutral	2	1.0	4.24	4.77	0.12
G5	neutral	2	10.0	5.62	6.35	0.13
G5	low	2	1.0	4.34	4.92	0.13
G5	low	2	10.0	8.06	9.07	0.13
G6	high	4		6.66	7.40	0.11
G6	neutral	4	1.0	6.76	7.46	0.10
G6	neutral	4	10.0	10.08	11.21	0.11
G6	low	4	1.0	6.69	7.40	0.11
G6	low	4	10.0	13.72	15.14	0.10

We numerically investigated the structural formation of dendrimer-based star polymers in an aqueous solution. Figure 6a shows a schematic illustration of dendrimers, with chemical modification of their outer surface. The blue and red lines denote dendrimers and linear polymers, respectively. In the following calculation, monomers of a dendrimer and outer polymer layers are electrically neutral ($z_i = 0$) as shown in eq 6. Figure 6b shows the snapshot of G5 dendrimers at three different temperatures such as $k_BT/\epsilon = 1.0$, 2.0, and 4.0. Here the length between nodes M_n and the length of polymer layers M_p are set to be $M_n = 4$ and $M_p = 15$, respectively. Figure 6b indicates that structure varies as a function of temperature. At lower temperature ($k_BT/\epsilon = 1.0$), the system becomes compact and looks like a spherical colloidal particles, and at higher temperature ($k_BT/\epsilon = 4.0$), the polymer layers spread outward.

In Figure 7, we show the results of the segment density distribution in order to clarify the internal structure of dendrimers with chemical modifications. Solid lines, dashed lines, and dotted lines denote the density distribution of all segments $n(r)$, dendrimer

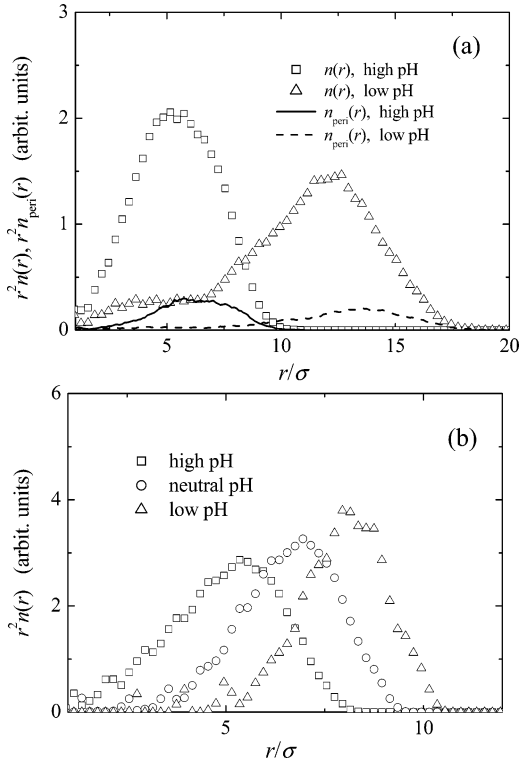

Figure 5. (a) H dependence of distribution functions $r^2n(r)$ and $r^2n_{peri}(r)$ of G5 dendrimers ($M_n = 4$). (b) pH dependence of distribution function $r^2n(r)$ of G7 dendrimers ($M_n = 1$).

Table 3. Gyration Radius R_g of G7 Dendrimers

pH	M_n	$(\kappa\sigma)^{-1}$	R_g/σ
high	2		6.53
neutral	2	10.0	10.03
low	2	10.0	12.69
high	1		5.10
neutral	1	10.0	6.66
low	1	10.0	7.95

skeletons $n_d(r)$, and polymer chains $n_p(r)$, respectively. Parts a and b of Figure 7 display the results with $k_BT/\epsilon = 1.0$ and 4.0, respectively. These results indicate that polymer chains attached to a dendrimer skeleton disperse into the molecule. Let us compare the calculated results in Figure 7 with core−shell model (spherical polymer brushes) described in ref 26. In eq 4 of ref 26, a radial density distribution function $n(r)$ is described as $n(r) \approx$ constant inside the dendrimer, $n(r) \propto r^{1/\nu-3}$ inside the PEG shell (ν is an exponent), and $n(r) = 0$ outside the star, respectively. In Figure 7, the calculated results on the density distribution function qualitatively agrees well with these profiles. Figure 7 also implies that such a spherical polymer brush picture is not perfect, because dendrimer skeltons and tethered polymer layers interpenetrate each other. It is a future problem to clarify the spatial distribution of dendrimer-based star polymers with much higher generations.

4. Effective Interaction between Dendrimers

It has been revealed that strongly charged polyelectrolytes show various characteristic behaviors.[27−30] Many studies on dendrimers have focused mainly on their structural formation, for example, the gyration radius and the validity of their dense shell (dense core) picture.[25,31−33] However, effective interaction between dendrimers has not yet been clarified yet. In this section, we study numerically the effective interaction between

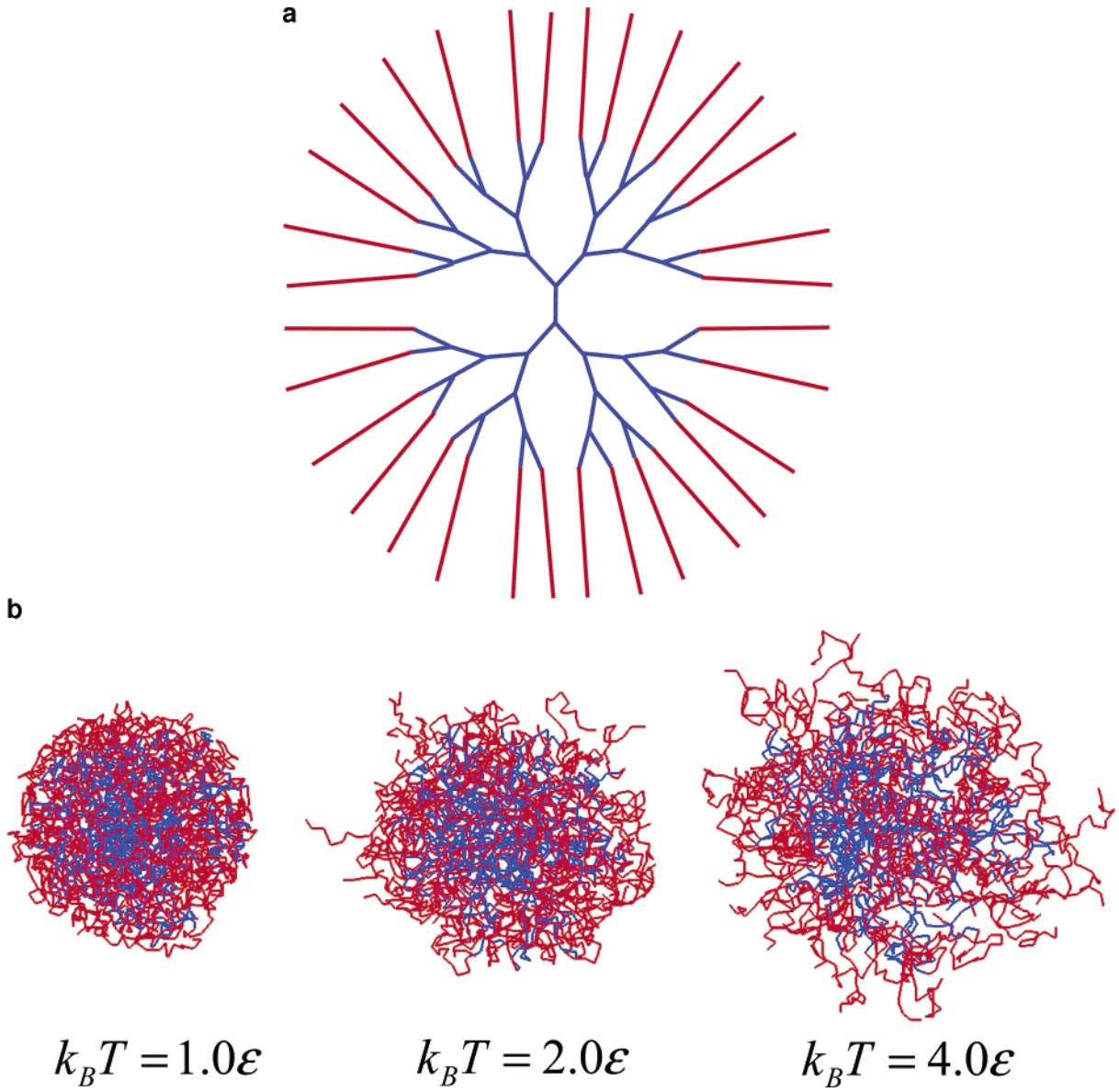

Figure 6. (a) Schematic picture of dendrimer-based star polymers. (b) Snapshot of dendrimer-based star polymers at three different temperatures ($k_BT/\epsilon = 1.0, 2.0, 4.0$).

dendrimer molecules in an aqueous solution. Recently, neutron scattering experiments have been performed on dendrimer systems, and it is necessary to know about the effective interaction between dendrimers to understand the scattering properties in concentrated systems.

In the following simulations, the implementation of the long-range Coulomb interaction requires special care to calculate the Coulomb sum written by

$$\frac{U_c'(r_{ij})}{k_BT} = \lambda_B \sum_{n_x=-\infty}^{\infty} \sum_{n_y=-\infty}^{\infty} \sum_{n_z=-\infty}^{\infty} \frac{z_i z_j}{|\boldsymbol{r_{ij}} + n_x L \boldsymbol{e_x} + n_y L \boldsymbol{e_y} + n_z L \boldsymbol{e_z}|} \quad (12)$$

where $\boldsymbol{e_x}$, $\boldsymbol{e_y}$, and $\boldsymbol{e_z}$ are unit vectors in the x, y, and z directions, respectively. We impose periodic boundary conditions in the x, y, and z directions, respectively, and the indices n_x, n_y, and n_z run over the periodic images of the systems. The long-range nature of the Coulomb interaction is numerically treated via the efficient method proposed by Lekner.[34] For an assembly of N charged particles in a central cubic cell of dimension L, the Coulomb force $\boldsymbol{F_i^{(c)}}$ exerted onto particle i by particle j, and by all repetitions of particle j in the periodic system, is

$$\boldsymbol{F_i^{(c)}} = q_i q_j \frac{q_i q_j}{4\pi\tilde{\epsilon}} \sum_j^{\text{all cells}} \frac{\boldsymbol{r_i} - \boldsymbol{r_j}}{|\boldsymbol{r_i} - \boldsymbol{r_j}|^3} \quad (13)$$

Because of x, y, and z symmetry, it is sufficient to consider only one component of the Coulomb force. For the x component of the force, we have

$$F_i^{(c),x} = \frac{q_i q_j 8\pi}{4\pi\tilde{\epsilon} L^2} \sum_{l=1}^{\infty} l \sin\left(2\pi l \frac{\Delta x}{L}\right) \sum_{m=-\infty}^{\infty} K_0 \left(2\pi l \sqrt{\left(\frac{\Delta y}{L} + m\right)^2 + \left(\frac{\Delta z}{L} + n\right)^2}\right) \quad (14)$$

Here, $\Delta x \equiv x_i - x_j$, $\Delta y \equiv y_i - y_j$, $\Delta z \equiv z_i - z_j$, and $K_0(z)$

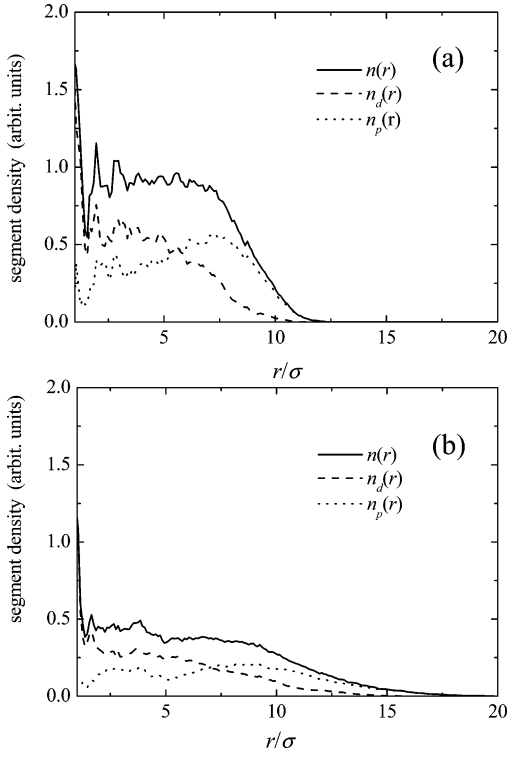

Figure 7. Profiles of density distribution functions $n(r)$, $n_d(r)$, and $n_p(r)$ of dendrimer-based star polymers: (a) at low temperature ($k_BT/\epsilon = 1.0$); (b) at high temperature ($k_BT/\epsilon = 4.0$).

is the modified Bessel function of zero order. To clarify the counterion size effect, we calculate the gyration radius of dendrimer R_g as a function of the diameter of counterions σ_c. We employ the interaction between monomers written by eq 4. In addition, the short-range repulsive contribution between a monomer and a counterion is given by

$$U_{mc}(r_{ij}) = \begin{cases} 4\epsilon\left[\left(\frac{\sigma_{mc}}{r_{ij}}\right)^{12} - \left(\frac{\sigma_{mc}}{r_{ij}}\right)^{6} - \left(\frac{\sigma_{mc}}{r_{mc}}\right)^{12} + \left(\frac{\sigma_{mc}}{r_{mc}}\right)^{6}\right] & \text{for } r_{ij} \le r_{mc} \\ 0 & \text{for } r_{ij} < r_{mc} \end{cases} \quad (15)$$

where σ_{mc} and r_{mc} are defined to be $\sigma_{mc} \equiv (\sigma + \sigma_c)/2$ and $r_{mc} \equiv 2^{1/6}\sigma_{mc}$, respectively. Similarly, the excluded-volume effect between counterions is given by

$$U_{cc}(r_{ij}) = \begin{cases} 4\epsilon\left[\left(\frac{\sigma_c}{r_{ij}}\right)^{12} - \left(\frac{\sigma_c}{r_{ij}}\right)^{6} - \left(\frac{\sigma_c}{r_{cc}}\right)^{12} + \left(\frac{\sigma_c}{r_{cc}}\right)^{6}\right] & \text{for } r_{ij} \le r_{cc} \\ 0 & \text{for } r_{ij} < r_{cc} \end{cases} \quad (16)$$

where r_{cc} is defined to be $r_{cc} \equiv 2^{1/6}\sigma_c$. The results on the gyration radius R_g with different size of counterions σ_c are shown in Table 4. The system size L is taken to be $L = 40\sigma$. Table 4 shows that the excluded volume of counterions leads to the expansion of the gyration radius of dendrimer molecules.

We study a pair of dendrimer molecules which are confined in a cubic box of length L. A pair of dendrimers are placed symmetrically along the body diagonal of the cube such that the center of the cube coincides with the center of mass of the two molecules. Their positions are denoted by $\boldsymbol{R_1}$ and $\boldsymbol{R_2}$ ($R \equiv |\boldsymbol{R_1} - \boldsymbol{R_2}|$). Furthermore, the box contains N_c counterions carrying an opposite charge, $-e$, when two dendrimer molecules are charged. Using molecular dynamics simulations, the effective force $\boldsymbol{F_i}$ acting on each dendrimer molecule i ($i = 1, 2$) is calculated. We consider both Coulomb (eq 13) and non-Coulomb parts to evaluate the effective force $\boldsymbol{F_i}$. Since by symmetry, $\boldsymbol{F_2} = -\boldsymbol{F_1}$, we project $\boldsymbol{F_i}$ onto the body diagonal defining

$$F(R) \equiv \frac{\boldsymbol{F_1} - \boldsymbol{F_2}}{2} \cdot \frac{(\boldsymbol{R_1} - \boldsymbol{R_2})}{|\boldsymbol{R_1} - \boldsymbol{R_2}|} \quad (17)$$

In eq 17, the effective interaction is repulsive when $F(R) > 0$, and vice versa. We perform stochastic MD simulations for a pair of fifth-generation dendrimers. Three different systems are considered such as (i) electrically neutral dendrimers, (ii) charged dendrimers in the medium with relative dielectric constant $\tilde{\epsilon}_r = 78.0$, and (iii) charged dendrimers with different dielectric constant $\tilde{\epsilon}'_r = \tilde{\epsilon}_r/10$. Results of the effective force $F(R)$ is shown in Figure 8a. In Figure 8, the system size L and the size of counterions σ_c are taken to be $L = 90\sigma$ and $\sigma_c = \sigma$, respectively. Open squares and open circles denote the results for neutral dendrimers and charged dendrimers ($\tilde{\epsilon}_r = 78$), respectively. In Figure 8a, the value of $2R_g$ is shown by vertical arrow. Both results

Table 4. Counterion Size Dependence on the Gyration Radius R_g of Fifth-Generation Dendrimers[a]

σ_c/σ	R_g/σ
1.0	7.24
0.8	6.42
0.6	5.73
0.4	5.46
0.2	5.34

[a] The length between branching point M_n is taken to be $M_n = 4$.

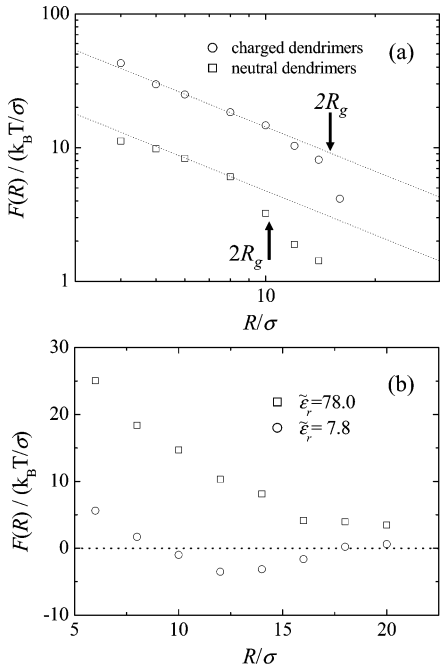

Figure 8. Effective force between dendrimers $F(R)$: (a) under different pH conditions; (b) under different strength of electrostatic couplings.

show that the effective force $F(R)$ decays as a power law such as

$$F(R) \sim \frac{1}{R^{\gamma}} \quad \text{for } R \ll 2R_g \tag{18}$$

with the exponent $\gamma = 1.0 \pm 0.1$. This implies that effective interaction between dendrimers $V(R)$ obeys $V(R) \propto -\log(R/\sigma)$ for $R \ll 2R_g$, and it decays more rapidly for $R > 2R_g$.

We also show the calculated results on the effective force with strong electrostatic couplings. In Figure 8b, the effect of strong electrostatic couplings is treated by smaller dielectric constant of the medium. Open squares and open circles denote the results for $\tilde{\epsilon}_r = 78$ and $\tilde{\epsilon}'_r = \tilde{\epsilon}_r/10$, respectively. Figure 8b demonstrates that the effective interaction between like-charged dendrimers becomes attractive when the electrostatic couplings is strong. It is interesting to address the possible mechanism for like-charged attraction shown in Figure 8b, because of its ion-penetrable nature associated with dendrimers. The physical origin of like-charged attraction is considered to be *fluctuation-induced attraction*, which is also observed in strongly charged polyelectrolytes with multivalent salt in solution.[35,36]

Conclusions

In conclusion, we have studied the structural formation of charged dendrimers and dendrimer-based star polymers by stochastic molecular dynamics simulations. Recent experiments[16] have shown that the structure and the gyration radius of dendrimers depend on the pH-condition and the ionic strength of the aqueous solution. Nisato et al.[17] have performed the SANS experiment on G8 PAMAM dendrimers, and concluded that the size of dendrimers does not change as a function of the charge density and ionic strength of the solvent. We have calculated the gyration radius, the density distribution function, and the structure factor of these systems under different pH conditions, ionic strengths, and number of generations (G5, G6, and G7). At a lower generation number, the gyration radius strongly depends on solvent properties. These results are in agreement with previous SANS experiments by Chen et al.,[16] and computer simulations by Welch and Muthukumar[23] and Lee et al.[24] At a higher generation number with a small free-volume, the pH dependence of the gyration radius decreases due to the steric effect between each segment. These tendencies suitably explain the recent SANS experiment performed on G8 dendrimers by Nisato et al.[17] We have also investigated the structural formation of a dendrimer-based star polymer in an aqueous solution, which is a model of sugar-substituted globular dendrimers[18] and PEG-dendrimers,[19,25] with many potential applications in biochemistry and medical science.

The effective interaction between dendrimer molecules is a critical issue for understanding scattering properties in an aqueous solution, especially for concentrated systems. The calculated results have shown that the effective force between dendrimers decays as a power law such as $F(R) \sim 1/R$. These results assert that dendrimers can be regarded as spherical colloidal particles with soft effective interaction. We also find that the effective interaction between like-charged dendrimers can be attractive when the electrostatic couplings is strong. These phenomena are reminiscent of DNA condensation, where negatively charged DNA molecules assembles via fluctuation-induced attraction.[28] These results give a deep insight into the physical description of the Coulomb screening effect on strongly charged soft matters[37−40] and motivate the development of novel, potential applications such as physical encapsulation of guest molecules, specific drug targeting, and pH-sensitive controlled release.

Acknowledgment. This work was supported in part by a Grant-in-Aid from the Japan Ministry of Education, Science, and Culture for Scientific Research. The authors thank the Supercomputer Center, Institute of Solid State Physics, University of Tokyo, for the use of the facilities.

References and Notes

(1) Fischer, M.; Vögtle, F. *Angew. Chem., Int. Ed. Engl.* **1999**, *38*, 884.
(2) Narayanan, V. V.; Newkome, G. R. *Top. Curr. Chem.* **1998**, *197*, 19.
(3) Zimmerman, S. C.; Wendland, M. S.; Rakow, N. A.; Zharov, I.; Suslick, K. S. *Nature (London)* **2002**, *418*, 399.
(4) Tomalia, D. A.; Baker, H.; Dewald, J.; Hall, M.; Kallos, G.; Martin, S.; Roeck, J.; Ryder, J.; Smith, P. *Polym. J. (Tokyo)* **1985**, *17*, 117.
(5) Krämer, M.; Stumbé, J.-F.; Türk, H.; Krause, S.; Komp, A.; Delineau, L.; Prokhorova, S.; Kantz, H.; Haag, R. *Angew. Chem., Int. Ed.* **2002**, *41*, 4252.
(6) Stiriba, S.-E.; Freym, H.; Haag, R. *Angew. Chem., Int. Ed.* **2002**, *41*, 1329.
(7) Patri, A. K.; Majoros, I. J.; Baker, J. R., Jr. *Curr. Opin. Chem. Biol.* **2002**, *6*, 466.
(8) Krause, W.; Hackmann-Schlichter, N.; Maier, F. K.; Müller, R. *Top. Curr. Chem.* **2000**, *210*, 261.
(9) Pistolis, G.; Malliaris, A.; Tsiourvas, D.; Peleos, C. M. *Chem.—Eur. J.* **1999**, *5*, 1440.
(10) Rosenfeldt, S.; Dingenouts, N.; Ballauff, M.; Werner, N.; Vögtle, F.; Lindner, P. *Macromolecules* **2002**, *35*, 8098.
(11) Rietveld, I. B.; Bouwman, W. G.; Baars, M. W. P. L.; Heenan, R. K. *Macromolecules* **2001**, *34*, 8380.
(12) Rathgebar, S.; Monkenbusch, M.; Kreitschmann, M.; Urban, V.; Brulet, A. *J. Chem. Phys.* **2002**, *117*, 4047.
(13) Ohshima, A.; Konishi, T.; Yamanaka, J.; Ise, N. *Phys. Rev. E* **2001**, *64*, 051808.
(14) Nisato, G.; Ivkov, R.; Amis, E. J. *Macromolecules* **1999**, *32*, 5895.
(15) Topp, A.; Bauer, B. J.; Klimash, J. W.; Spindler, R.; Tomalia, D. A.; Amis, E. J. *Macromolecules* **1999**, *32*, 7226.
(16) Chen, W.; Tomalia, D. A.; Thomas, J. L. *Macromolecules* **2000**, *33*, 9169.
(17) Nisato, G.; Ivkov, R.; Amis, E. J. *Macromolecules* **2000**, *33*, 4172.
(18) Aoi, K.; Itoh, K.; Okada, M. *Macromolecules* **1995**, *28*, 5391.
(19) Liu, M.; Kono, K.; Fréchet, J. M. J. *J. Polym. Sci., Part A: Polym. Chem.* **1999**, *37*, 3492.
(20) Grest, G. S.; Kremer, K. *Phys. Rev. A* **1986**, *33*, 3628.
(21) Lee, I.; Athey, B. D.; Wetzel, A. W.; Meixner, W.; Baker, J. R., Jr. *Macromolecules* **2002**, *35*, 4510.
(22) Lyulin, A. V.; Davies, G. R.; Adolf, D. B. *Macromolecules* **2000**, *33*, 3294.
(23) Welch, P.; Muthukumar, M. *Macromolecules* **1998**, *31*, 5892.
(24) Lee, I.; Athey, B. D.; Wetzel, A. W.; Meixner, W.; Baker, J. R. *Macromolecules* **2002**, *35*, 4510.
(25) Timoshenko, E. G.; Kuznetsov, Y. A.; Connolly, R. *J. Chem. Phys.* **2002**, *117*, 9050.
(26) Hedden, R. C.; Bauer, B. J. *Macromolecules* **2003**, *36*, 1829.
(27) Bloomfield, V. A. *Biopolymers* **1991**, *31*, 1471.
(28) Netz, R. R.; Joanny, J.-F. *Macromolecules* **1999**, *32*, 9026.
(29) Terao, T.; Nakayama, T. *Phys. Rev. E* **2001**, *63*, 041401.
(30) Grosberg, A. Y.; Nguyen, T. T.; Shklovskii, B. I. *Rev. Mod. Phys.* **2002**, *74*, 329 and references therein.
(31) For example: Zook, T. C.; Pickett, G. T. *Phys. Rev. Lett.* **2003**, *90*, 015502.
(32) Likos, C. N.; Rosenfeldt, S.; Dingenouts, N.; Ballauff, M.; Lindner, P.; Werner, N.; Vögtle, F. *J. Chem. Phys.* **2002**, *117*, 1869.

(33) Karatasos, K.; Adolf, D. B.; Davies, G. R. *J. Chem. Phys.* **2001**, *115*, 5310.
(34) Lekner, J. *Physica A* **1991**, *176*, 485.
(35) Terao, T.; Nakayama, T. *J. Phys.: Condens. Matter* **2000**, *12*, 5169.
(36) Terao, T.; Nakayama, T. *Colloids Surf. A* **2001**, *182*, 299.
(37) Terao, T.; Nakayama, T. *Phys. Rev. E* **2002**, *65*, 021405.
(38) Terao, T. *Phys. Rev. E* **2002**, *66*, 046707.
(39) Israelachivili, J. *Intermolecular and Surface Forces*, 2nd ed.; Academic Press: London, 1992.
(40) Terao, T.; Nakayama, T. *Phys. Rev. E* **1999**, *60*, 7157.

MA030349H